Peer-reviewed version available at *Metals* **2019**, *9*, 252; doi:10.3390/met9020252

Article

Electronic structure calculations of oxygen atom transport energetics in the presence of screw dislocations in tungsten

Yue Zhao [1,2,3], Lucile Dezerald [2,3]*, and Jaime Marian [1,4]

1 Department of Materials Science and Engineering, University of California Los Angeles, Los Angeles, CA 90095, USA; zy111693@ucla.edu ; jmarian@g.ucla.edu
2 Department of Metallurgy, Materials Science and Engineering, Institut Jean Lamour, Université de Lorraine, Campus ARTEM, Allée André Guinier, F-54011 Nancy, France, lucile.dezerald@univ-lorraine.fr
3 Laboratory of Excellence on Design of Alloy Metals for low-mAss Structures (DAMAS), Universitat de Lorraine, 57073 Metz, France
4 Department of Mechanical and Aerospace Engineering, University of California Los Angeles, Los Angeles, CA 90095, USA
* Correspondence: lucile.dezerald@univ-lorraine.fr; Tel.: +33-3-72-74-26-81

Abstract: Plastic flow in body-centered cubic (bcc) alloys is governed by the thermally-activated screw dislocation motion. In bcc interstitial solid solutions, solute diffusion can occur at very fast rates owing to low migration energies and solute concentrations. Under mechanical loading, solutes may move on the same or similar time scale as dislocations glide, even at low temperatures, potentially resulting in very rich co-evolution processes that may have important effects in the overall material response. It is therefore important to accurately quantify the coupling between interstitial impurities and dislocations, so that larger-scale models can correctly account for their (co)evolution. In this paper, we use electronic structure calculations to obtain the energetics of oxygen diffusion under stress and its interaction energy with screw dislocation cores in bcc tungsten. We find that oxygen atoms preferentially migrate from tetrahedral to tetrahedral sites with an energy of 0.2 eV. This energy couples only weakly to hydrostatic and deviatoric deformations, with activation volumes of less than 0.02 and $0.2b^3$, respectively. The strongest effect is found for the inelastic interaction between O atoms and screw dislocation cores, which leads to attractive energies on the order of 1.5 eV and a structural transformation of the screw dislocation core from an 'easy' to a 'hard' core configuration.

Keywords: W-O alloy, interstitial solid solution, screw dislocations, solute diffusion, stress coupling

1. Introduction

Refractory transition metals such as those in groups V and VI of the periodic table are an important class of materials due to their high-temperature strength and corrosion resistance [1–3]. However, they typically display poor low-temperature fracture toughness and must be alloyed with other transition metal elements to improve their ductility. For example, in the case of body-centered cubic (bcc) W, W-Re alloys have been shown to lower the ductile-to-brittle transition temperature by up to hundreds of degrees [4], resulting in commercially viable alloys. Interstitial impurities, however, are known to produce marked increases in the ductile-to-brittle transition temperature (DBTT) of polycrystalline specimens [5]. Specifically, oxygen is seen to lower both the tensile and yield strengths, while promoting intergranular fracture at concentrations as low as 30 appm. In single crystals, the effect is less pronounced, although some evidence suggests a hardening effect at low temperatures [6–8]. As well, oxygen is known to be involved in dynamic strain aging in tungsten-based systems deformed within a certain strain rate and temperature window [9,10]. In principle, O is soluble in tungsten up to the formation of the line compound WO_2 at 66.7 at.% [11], although embrittling second phases have been seen to form at grain boundaries at only a few appm of concentration [12]. In

Peer-reviewed version available at Metals 2019, 9, 252; doi:10.3390/met9020252

single crystals, the effect can be isolated to dislocation core/solute interactions, particularly screw dislocations, as they are known to control plasticity in bcc metals at low-to-intermediate temperatures [13–15]. By its very nature, this interaction can only be studied using atomistic resolution methods to describe the highly nonlinear lattice deformations around the dislocation core. At the same time, the method must capture the essential details of W-O chemistry, which may become important in non-dilute conditions. These restrictions point to density functional theory (DFT) as the technique of choice to investigate dislocation-O interactions in W.

Numerous studies have been performed on dislocation core/solute interactions using DFT calculations. For substitutional solutes, several works including face and body-centered materials exist [16–23], while for interstitial impurities recent calculations including a number of different solutes in Fe have been recently published [24–26], as well as dislocation-C interactions in bcc transition metals [27]. These calculations show that solute atoms stabilize the hard core configuration of a screw dislocation when the solutes are placed inside the triangular prism formed by the the three $\langle 111 \rangle$ atomic rows enclosing the dislocation core.

Interestingly, despite its technological importance, no DFT studies have been performed on the interactions between dislocation and O in W. The primary objective of this work is to investigate the interactions of oxygen interstitial solute with screw dislocations in bcc W. These interactions can be categorized as *long-range*, i.e. elastic interactions affecting the diffusive behavior of oxygen atoms in the presence of dislocations, or *short-range*, i.e. local binding of chemical nature between dislocation cores and impurities. Consequently, here we study first the dependence on stress of the diffusivity of O interstitials atoms in bulk W, followed by the calculation of interaction energies between O atoms and screw dislocation cores. We end the paper with a discussion and the conclusions.

2. Computational details

All DFT calculations were carried using the VASP code [28]. Calculations were performed using the *projector augmented wave* (PAW) [29,30] pseudopotential scheme within the Perdew-Burke-Ernzerhof (PBE) generalized gradient approximation and a 400 eV kinetic-energy cutoff. The Hermite-Gaussian scheme was employed, with a smearing of 0.2 eV for electronic occupation. Structure relaxation was performed until the forces on all the atoms are less than 2×10^{-2} eV/Å.

2.1. O solution and migration energies under strain

Calculations of O-atom solution and migration energy in bulk W were performed using 250 atoms bcc supercells with a 4×4×4 *k*-point grid. The migration barrier was calculated between two neighboring configurations of lowest energy (tetrahedral sites in the present case) using the

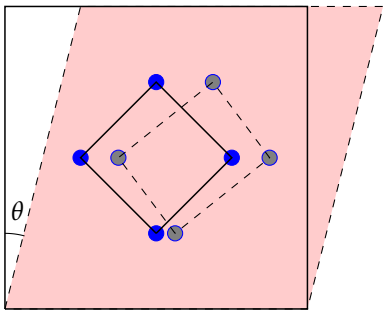

Figure 1. Illustration of the distortion of tetrahedral→tetrahedral paths under shear deformation. The undeformed path becomes stretched along two directions and compressed along the other two. θ represents the shear angle (refer to Sec. 2).

nudged elastic band (NEB) method as implemented in VASP. O migration in bulk W under strain was investigated by applying the following transformation matrices to the supercell lattice vectors:

$$\boldsymbol{a}' = (\boldsymbol{\varepsilon} + \boldsymbol{I})\,\boldsymbol{a} \tag{1}$$

where $\boldsymbol{a}'$ are the deformed lattice vectors, $\boldsymbol{\varepsilon}$ is the applied strain tensor, $\boldsymbol{I}$ is the identity tensor, and $\boldsymbol{a}$ are the undeformed lattice vectors. The undeformed configuration is expressed in a canonical cartesian reference system with $\boldsymbol{a_1} \equiv [a_0\ 0\ 0]$, $\boldsymbol{a_2} =\equiv [0\ a_0\ 0]$, and $\boldsymbol{a_3} \equiv [0\ 0\ a_0]$, where $a_0 = 3.186$ Å is the lattice parameter of W calculated with the pseudopotential employed here. Two different strain tensors were applied for the simulations:

(i) Hydrostatic strain:

$$\boldsymbol{\varepsilon} = \begin{bmatrix} \epsilon & 0 & 0 \\ 0 & \epsilon & 0 \\ 0 & 0 & \epsilon \end{bmatrix}$$

(ii) Volume-conserving shear:

$$\boldsymbol{\varepsilon} = \begin{bmatrix} 0 & \gamma/2 & 0 \\ \gamma/2 & 0 & 0 \\ 0 & 0 & 0 \end{bmatrix}$$

where ϵ and γ are the applied dilatational and shear strains, respectively.Positive values of ϵ are taken to represent tensile deformations. Note that in the limit of small deformations, the volumetric strain $\varepsilon_v = \Delta V/V \approx \mathrm{Tr}(\boldsymbol{\varepsilon}) = 3\epsilon$. It is assumed that in the limit of small deformations $\gamma = \tan\theta$ with θ the shear angle as defined in Figure 5. Note that shear deformation turns a symmetric cubic cell into a monoclinic one, which results in a shortening of certain tetrahedral→tetrahedral paths and in extension of others, as illustrated in Figure 1. This is equivalent to applying negative shear strain and, consequently, we have investigated both reaction paths when calculating O migration in sheared bcc W.

2.2. Dislocation-O interactions

Simulations of dislocation-O interactions were performed using 135 W-atom supercells containing a $a_0/2[111]$ screw dislocation dipole as is typically used for such simulations [31,32], with a $1\times2\times16$ k-point grid. The cell was first relaxed in the absence of O to determine the reference energy for dislocation-solute interactions. This results in an *easy*, non-degenerate core configuration, consistent with a number of other independent DFT calculations [31–36]. Solute atoms were subsequently inserted in various tetrahedral sites around the dislocation center, as shown in Figure 7. The use of periodic boundary conditions along the [111] direction when placing an O atom in the supercell results in a row of atoms separated by a distance of $1b$ (equal to the thickness of the box). We tested the impact of using such thin specimens by repeating one of the calculations with a thickness of $2b$ finding no effect on the final numbers.

3. Results

3.1. Oxygen atom stability in bulk tungsten

Oxygen stability in bulk W is evaluated by separately inserting one oxygen atom in tetrahedral and octahedral sites of a bulk W bcc structure. Figure 2 shows the geometric location of the interstices in a bcc unit cell. The solution energy H_s (heat of solution) is defined as:

$$H_s = E_{\text{W-O}} - E_{\text{W}} - \mu_{\text{O}} \tag{2}$$

Preprints (www.preprints.org) | NOT PEER-REVIEWED | Posted: 4 January 2019 doi:10.20944/preprints201901.0033.v1

Peer-reviewed version available at Metals 2019, 9, 252; doi:10.3390/met9020252

where $E_{\text{W-O}}$ and E_{W} are, respectively, the energies of a W cell with and without O, and μ_{O} is the energy of an isolated O atom. We find a solution energies of -2.32 eV and -2.63 eV for for octahedral and tetrahedral sites, respectively. While this is consistent with recent studies in W-O [37], it deviates from what is commonly found for other bcc metals, where octahedral sites are more stable for interstitial impurities[1] [26,38]. The reasons behind this behavior appear to be related to the overlap of electron charge densities, which leads to a more stable bonding configuration when O is at a tetrahedral location [37].

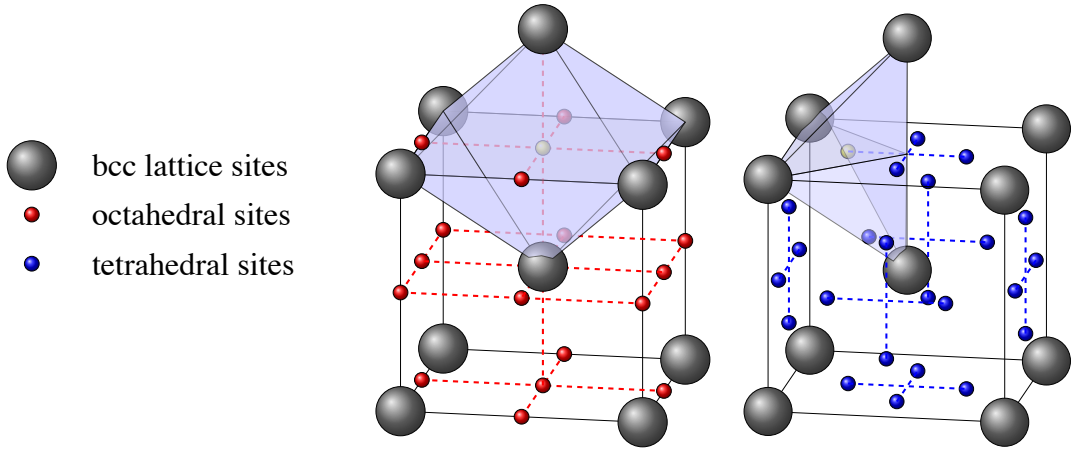

Figure 2. Elementary bcc lattice cell showing octahedral and tetrahedral interstitial sites. As a guide to the eye, the figures show a shaded octahedron and tetrahedron with the interstitial site highlighted in their respective centers. In principle, transitions may occur between any two nearest neighbor interstitial sites.

Next, we study the dependence of H_s with strain applied in the manner described in Sec. 2.1. The results are shown in Figure 3, clearly indicating a strong coupling to volumetric strain but an almost negligible one to shear deformation. Assuming a linear dependence with ε, we find:

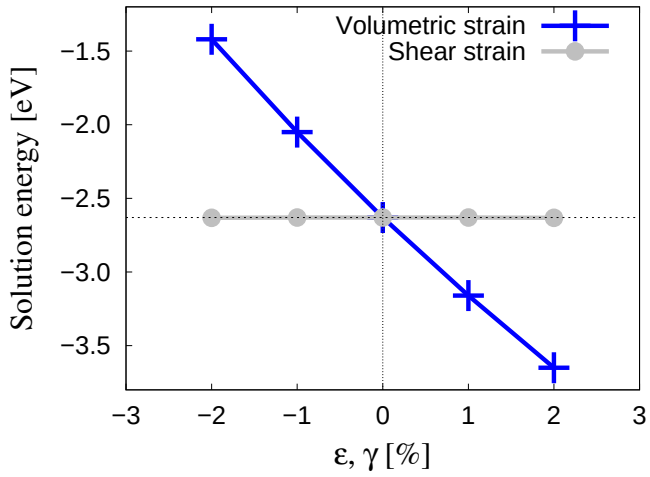

Figure 3. Variation of the heat of solution of tetrahedral O as a function of volumetric, ε, and shear, γ, strain.

[1] Consistent with an octahedral volume of $V_{\text{oct}} = a_0^3/3$, versus a tetrahedral one of $V_{\text{tet}} = a_0^3/12$.

$$H_s(\epsilon) = -2.63 - 57.7\epsilon = -2.63 - \frac{57.7p}{3B_W} \text{ [eV]}$$

where $p = 1/3\,\mathrm{Tr}(\boldsymbol{\sigma})$ is the pressure, B_W is the bulk modulus of pure W. For a value of $B_W = 308.5$ GPa calculated using the same pseudopotential, we obtain the dependence of the heat of solution with stress:

$$H_s(\boldsymbol{\sigma}) = -2.63 - 9.98 \times 10^{-3} p = -2.63 - 3.33 \times 10^{-3}(\sigma_{xx} + \sigma_{yy} + \sigma_{zz}) \quad (3)$$

with p and the components of $\boldsymbol{\sigma}$ expressed in MPa.

We have also calculated the formation energy of an O atom at a vacant site and have obtained a value of -3.47 eV. This implies binding energies in excess of 2.0 eV (given a vacancy formation energy of 3.20 eV for the present pseudopotential, in agreement with several works [35,39,40]). This association with a vacancy results in a *substitutional* O atom, which, as earlier DFT calculations have shown for other interstitial solutes [41], effectively immobilizes it, thus changing the character of its contribution to the kinetic evolution of the system.

3.2. Oxygen migration in bulk tungsten

The migration barrier between two neighboring tetrahedral sites was evaluated using the NEB method (refer to Sec. 2). In the absence of applied strain, we found a value of 0.20 eV for the migration energy of O in W, in good agreement with the 0.17 eV obtained by Alkhamees *et al.* [37] and in contrast with values over 0.3 eV for octahedral→octahedral transitions by the same authors. This is also in concordance with both DFT and semi-empirical interatomic potential calculations of O migration in other bcc metals that consistently yield larger values for the octahedral→octahedral jump [42–45]. Here, we expand on the calculations by Alkhamees *et al.* by studying the dependence of the migration barrier on hydrostatic and shear strain. Results for tensile and compressive strains are shown in Figure 4a. The results reveal a linear dependence of the migration energy barrier on hydrostatic strain, as shown in Fig. 4b, with a proportionality constant of $k_{\mathrm{hydro}} = 2.74$ eV. This implies a constant activation volume, which for this transition can be calculated as:

$$\Omega_{\mathrm{hydro}} = \frac{k_{\mathrm{hydro}}}{3B_W}$$

For the value of B_W given above, $\Omega_{\mathrm{hydro}} = 0.47$ Å$^3 = 0.022b^3$.

The dependence of the migration energy on shear strain is shown in Figure 5a. As mentioned above, shortened and lengthened paths (refer to Fig. 1) are simply manifestations of the sign of the applied shear strain and thus we show all the calculations on the same plot. In the case of shear, the activation volume is defined as:

$$\Omega_{\mathrm{shear}} = \frac{k_{\mathrm{shear}}}{\mu_W}$$

where, from the results in Fig. 5b, $k_{\mathrm{shear}} = 3.70$ eV is the proportionality constant and $\mu_W = 160.2$ GPa is the shear modulus for the current pseudopotential. With this, $\Omega_{\mathrm{shear}} = 3.98$ Å$^3 = 0.19b^3$ is obtained.

It is worth noting that, while the reaction path in Figs. 4a and 5a is show as projected along the rectilinear path joining two first-nearest neighbor tetrahedral sites, the actual trajectory is curved, as can be seen in Figure 6 for the unstrained case. The figure also shows the positions of two octahedral sites lying on the same plane as the tetrahedral ones for the (001) plane.

3.3. Dislocation-oxygen interaction in tungsten

The calculations carried out in the previous section allow us to couple solute diffusion to the dislocation elastic fields. However, there also exists an *inelastic* interaction that takes place when the solute atom is found close to the dislocation core. There, *chemical* effects of local nature dominate over long-range elastic interactions and it is therefore important to quantify them. Next we calculate the

Preprints (www.preprints.org) | NOT PEER-REVIEWED | Posted: 4 January 2019 doi:10.20944/preprints201901.0033.v1

Peer-reviewed version available at Metals 2019, 9, 252; doi:10.3390/met9020252

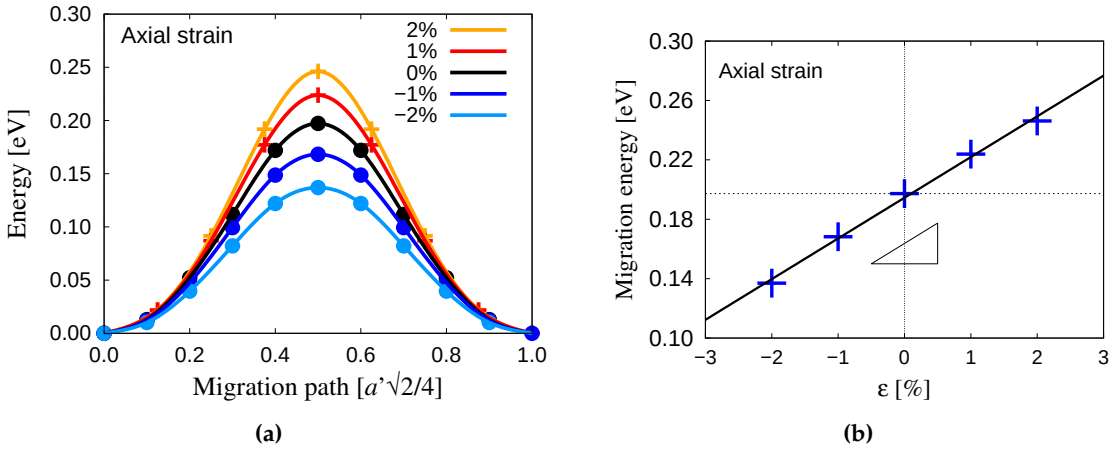

Figure 4. (a) Tetrahedral→tetrahedral oxygen migration energy path in bulk W calculated with DFT between two neighboring tetrahedral sites under hydrostatic strain. a' is defined in eq. (1). (b) Migration energy barrier under uniform axial strain. The black line represents a least-squares linear fit, from whose slope (black triangle) the activation volume can be calculated.

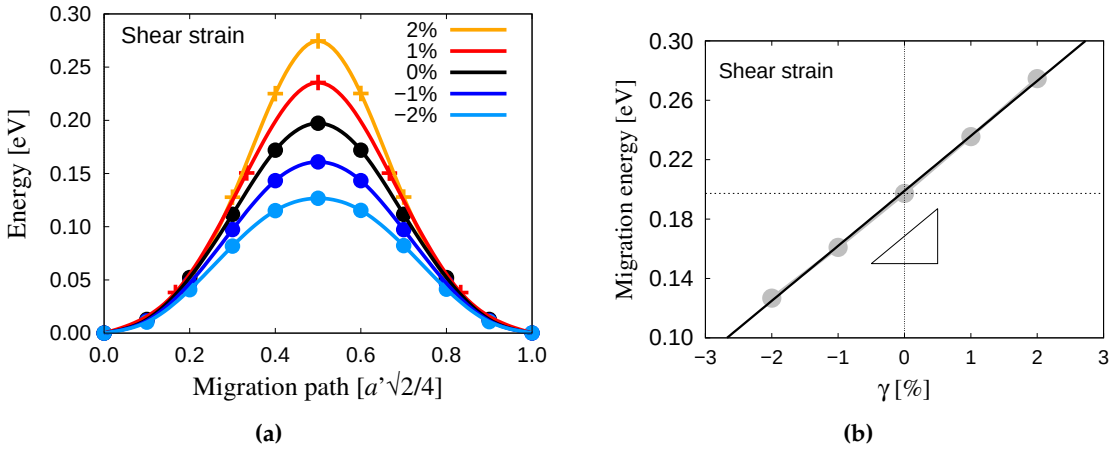

Figure 5. (a) Tetrahedral→tetrahedral oxygen migration energy path in bulk W calculated with DFT between two neighboring tetrahedral sites under shear strain. (b) Migration energy barrier under shear strain. The black line represents a least-squares linear fit, from whose slope (black triangle) the activation volume can be calculated.

Preprints (www.preprints.org) | NOT PEER-REVIEWED | Posted: 4 January 2019 doi:10.20944/preprints201901.0033.v1

Peer-reviewed version available at Metals 2019, 9, 252; doi:10.3390/met9020252

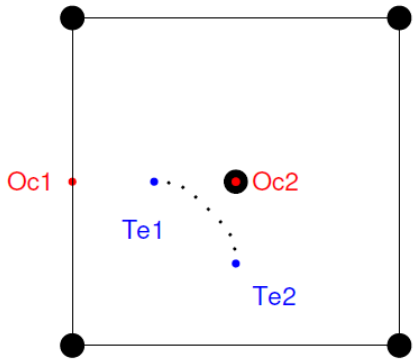

Figure 6. Migration path of an oxygen atom along two tetrahedral sites on a (001) plane under zero strain showing two neighboring octahedral sites for reference. The trajectory follows a curved path arched towards the closest octahedral site.

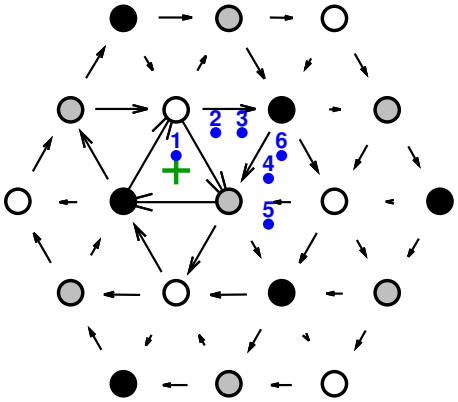

Figure 7. Location of the six nearest tetrahedral sites (blue points) to the geometric center of a screw dislocation core (green cross) before the relaxation of the dislocation-O system with DFT. The dislocation is in an easy core configuration. The arrows represent the amplitude of atomic displacements along the $\langle 111 \rangle$ direction (normal to the image) induced by the presence of the dislocation.

interaction energies between oxygen atoms and $\frac{a_0}{2}\langle 111 \rangle$ screw dislocation cores in W using balanced dislocation dipole geometries. First, the interaction energy is defined as:

$$E_{\mathrm{i}} = \frac{1}{2}\left(E^{\mathrm{dislo}}_{\mathrm{W\text{-}O}} - E^{\mathrm{dislo}}_{\mathrm{W}}\right) + \left(E^{\mathrm{bulk}}_{\mathrm{W}} - E^{\mathrm{bulk}}_{\mathrm{W\text{-}O}}\right) \tag{4}$$

where $E^{\mathrm{dislo}}_{\mathrm{W\text{-}O}}$ and $E^{\mathrm{dislo}}_{\mathrm{W}}$ are the energies of the dislocated cells with and without oxygen atoms, respectively, while $E^{\mathrm{bulk}}_{\mathrm{W\text{-}O}}$ and $E^{\mathrm{bulk}}_{\mathrm{W}}$ are the energies of bulk W with and without O atoms. The $1/2$ factor is used to account for the existence of two dislocations in the simulation cell. We study configurations with oxygen atoms at each of the six nearest tetrahedral sites to the dislocation core, as illustrated in Figure 7. Upon relaxation, an interesting phenomenon is observed. We find that the presence of oxygen leads to the reconstruction of the dislocation core into the so-called *hard* core configuration in five out of the six cases considered, as shown in Figure 8a. While the hard core is in generally a higher energy configuration for screw dislocations in bcc metals [31,32,34], oxygen stabilizes it in a manner similar to what has been observed for C atoms in several bcc metals [26,46]. Figure 8b shows that, in one of the six cases we tested, the dislocation core remained in an easy core configuration after relaxation in the presence of O. The relaxed position of the oxygen atoms is also shown in the

Preprints (www.preprints.org) | NOT PEER-REVIEWED | Posted: 4 January 2019 doi:10.20944/preprints201901.0033.v1

Peer-reviewed version available at Metals 2019, 9, 252; doi:10.3390/met9020252

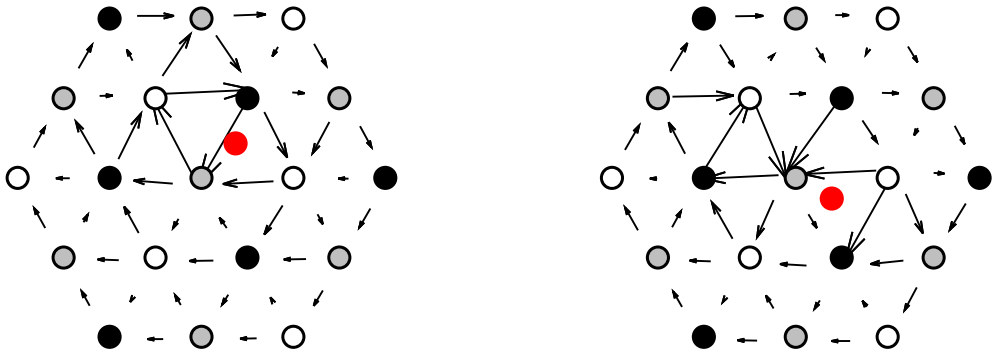

(a) 1st-4th NN, 6th NN. **(b)** 5th NN.

Figure 8. Final configurations for the dislocation core-O system as a function of the initial O atom position (shown in Fig. 7). (a) The resulting core structure is a *hard* core. (b) The resulting core structure is an *easy* core.

figure as a red dot. Except for the atom in position 5, which remains in place after relaxation and for which the easy core configuration is maintained, all other atoms are found in position 4 after relaxation, regardless of their original location.

The values of E_i obtained in each case are given in Table 1. We find that all the calculated energies are negative, ranging between -1.20 and -1.91 eV, indicating a strong attraction between O atoms and the dislocation core. Despite resulting in the same final configuration, the calculated energies for cases 1-4 and 6 depend on the initial position of the O atom (albeit slightly). The interaction energy for case number 5 –where the dislocation retains its easy core configuration and the O atom remains in its original site– was found to be the lowest of all the cases considered.

Table 1. Dislocation-O atom interaction energy for the six tetrahedral configurations considered in Fig. 7, showing the final oxygen state after relaxation.

Initial location	Final location	Interaction energy (eV)
1	4	-1.91
2	4	-1.81
3	4	-1.53
4	4	-1.83
5	5	-1.20
6	4	-1.83

This is consistent with calculated elastic distortions of near 40% in the atoms bounding the tetrahedral site around the solute. The effect of the dislocation core is to accommodate these distortions caused by the O atom into its own displacement field, resulting in energetically very favorable configurations. However, the deformation field due to the solute decays very rapidly, such that it is almost zero at second nearest neighbor positions from it.

4. Discussion

The present calculations are intended to provide quantitative support for mesoscale models of dislocation-solute coevolution, ultimately designed to explore the mechanisms behind serrated flow in bcc metals. As such, two types of interactions must be characterized, long and short range, of elastic

and inelastic nature, respectively. The former affects tetrahedral→tetrahedral oxygen atom migration under dislocation stress fields via an Arrhenius expression of the following type:

$$\nu\left(T,\boldsymbol{\sigma}(\boldsymbol{r})\right)=\nu_0\exp\left(-\frac{\Delta H_a(\boldsymbol{\sigma}(\boldsymbol{r}))}{kT}\right) \tag{5}$$

where ν_0 is an attempt frequency, ΔH_a is the *activation* enthalpy for the diffusive jump and k and T are Boltzmann's constant and the absolute temperature, respectively. The activation enthalpy has several contributions:

$$\Delta H_a = E_m + \Delta H_s - W_m$$

with:

$$\begin{aligned} E_m &= 0.20\ \text{eV} \\ \Delta H_s &= H_s(\boldsymbol{\sigma}(\boldsymbol{r_2})) - H_s(\boldsymbol{\sigma}(\boldsymbol{r_1})) \\ W_m &= \boldsymbol{\sigma}(\boldsymbol{r_1}) : \boldsymbol{\Omega} \end{aligned}$$

$\boldsymbol{\Omega}$ is the activation volume tensor obtained in this work:

$$\boldsymbol{\Omega}=\frac{\partial E_m}{\partial \boldsymbol{\sigma}}=\begin{bmatrix}\Omega_{\text{hydro}} & \Omega_{\text{shear}} & \Omega_{\text{shear}}\\ \Omega_{\text{shear}} & \Omega_{\text{hydro}} & \Omega_{\text{shear}}\\ \Omega_{\text{shear}} & \Omega_{\text{shear}} & \Omega_{\text{hydro}}\end{bmatrix}=b^3\begin{bmatrix}0.022 & 0.190 & 0.190\\ 0.190 & 0.022 & 0.190\\ 0.190 & 0.190 & 0.022\end{bmatrix} \tag{6}$$

In eq. (5), $\boldsymbol{\sigma}$ represents the stress tensor defined at spatial points $\boldsymbol{r_1}$ and $\boldsymbol{r_2}$ representing the initial and final coordinates of the O atom transition, including all contributions, e.g. applied external stress, stresses from other dislocation segments, etc.

For its part, the inelastic effect occurs locally at the dislocation core, where elasticity is no longer suitable to capture the dislocation-oxygen interaction. A strong dislocation core-O atom attraction is found, as evidenced by interaction energies in excess of 1.5 eV. While this is generally consistent with existing DFT calculations of small interstitial impurities and screw dislocation cores in the literature [26,47,48], it must also be kept in mind that these calculations are done for dislocation segments of length $1b$, and thus a contribution to E_i from periodic image O-O interactions cannot be discounted. By way of example, for the first case shown in Table 1, the interaction energies found between cells with thicknesses of $1b$ and $2b$ were -1.9 and -1.6 eV respectively . In any case, however, in view of the numbers calculated here, it is reasonable to assume that the inelastic effect will dominate over the elastic one at least in terms of long-term evolution. Additionally, when O atoms decorate the dislocation line in the manner created by the DFT calculations presented here, the core structure is seen to stabilize in the hard core configuration. Whether this is the case for longer dislocation segments ($>2b$), i.e. for smaller O-atom linear densities, is not clear at present, although previous calculations in bcc metals point to similar transformations [22,24,26], which may suggest the existence of some kind of universal effect.

Both of the above effects must be included in simulations of microstructural evolution to study the fundamental mechanisms behind interstitial solid solution softening/hardening or dynamic strain aging. We have some experience developing this type of models for substitutional alloys [49], which allow us to push the length and timescale envelope to experimentally-meaningful levels. The coupling of the energetics obtained in this work and mesoscopic models of dislocation-solute evolution is the subject of an ongoing effort which will be published in future studies..

5. Conclusions

- We have conducted electronic structure calculations of the fundamental energetics of oxygen atoms in tungsten, including the heat of solution, migration energies, activation volumes, and interaction energy with screw dislocation cores.

- Oxygen atoms are preferentially found in tetrahedral lattice sites, with solution energies of -2.63 eV. The *substitutional* heat of solution (an O atom associated with a vacant site) was found to be -3.47 eV.
- The nominal migration energy for the tetrahedral$\rightarrow$tetrahedral transition is 0.20 eV. This energy is modified by stress according to activation volumes of $0.02b^3$ and $0.19b^3$ for volumetric and shear deformations, respectively.
- The interaction energy between a screw dislocation of an O atom depends slightly on the relative position of the O atom but it is found to be in excess of 1.5 eV (attractive). We find that this is due to the accommodation of the large local distortions induced by the O atom in the lattice, which is seen to lead to a core reconstruction from the easy to the hard configuration.
- These calculations will serve to parameterize mesoscale models of material deformation by dislocation slip.

References

1. Tietz, T.E.; Wilson, J.W. Behavior and properties of refractory metals **1965**.
2. Davis, J.R. *Alloying: understanding the basics*; ASM international, 2001.
3. Lassner, E.; Schubert, W.D. Tungsten alloys. In *Tungsten*; Springer, 1999; pp. 255–282.
4. Lassner, E.; Schubert, W.D. Properties, Chemistry, Technology of the Element, Alloys, and Chemical Compounds. *Vienna University of Technology, Vienna, Austria, Kluwer* **1999**, pp. 124–125.
5. Stephens, J.R. Effects of interstitial impurities on the low-temperature tensile properties of tungsten. Technical report, NATIONAL AERONAUTICS AND SPACE ADMINISTRATION CLEVELAND OH LEWIS RESEARCH CENTER, 1964.
6. Ulitchny, M.; Gibala, R. The effects of interstitial solute additions on the mechanical properties of niobium and tantalum single crystals. *Journal of the Less Common Metals* **1973**, *33*, 105–116.
7. Stein, D.; Low Jr, J. Effects of orientation and carbon on the mechanical properties of iron single crystals. *Acta Metall.* **1966**, *14*, 1183–1194.
8. Smialek, R.; Mitchell, T. Interstitial solution hardening in tantalum single crystals. *Philos. Mag.* **1970**, *22*, 1105–1127.
9. Baird, J. The effects of strain-ageing due to interstitial solutes on the mechanical properties of metals. *Metall. Rev.* **1971**, *16*, 1–18.
10. Das, J.; Sankaranarayana, M.; Nandy, T. Serrated flow behavior in tungsten heavy alloy. *Mater. Sci. Eng., A* **2015**, *646*, 75–81.
11. Wells, A.F. *Structural inorganic chemistry*; Oxford university press, 2012.
12. Stephens, J.R. Effect of oxygen on mechanical properties of tungsten. Technical report, NATIONAL AERONAUTICS AND SPACE ADMINISTRATION CLEVELAND OH LEWIS RESEARCH CENTER, 1963.
13. Cottrell, A.H.; Bilby, B. Dislocation theory of yielding and strain ageing of iron. *Proceedings of the Physical Society. Section A* **1949**, *62*, 49.
14. Vitek, V.; Perrin, R.; Bowen, D. The core structure of 1/2 (111) screw dislocations in bcc crystals. *Philos. Mag.* **1970**, *21*, 1049–1073.
15. Clouet, E.; Garruchet, S.; Nguyen, H.; Perez, M.; Becquart, C.S. Dislocation interaction with C in α-Fe: A comparison between atomic simulations and elasticity theory. *Acta Mater.* **2008**, *56*, 3450–3460.
16. Trinkle, D.R.; Woodward, C. The chemistry of deformation: How solutes soften pure metals. *Science* **2005**, *310*, 1665–1667.
17. Medvedeva, N.; Gornostyrev, Y.N.; Freeman, A. Solid solution softening and hardening in the group-V and group-VI bcc transition metals alloys: First principles calculations and atomistic modeling. *Phys. Rev. B: Condens. Matter* **2007**, *76*, 212104.
18. Romaner, L.; Ambrosch-Draxl, C.; Pippan, R. Effect of rhenium on the dislocation core structure in tungsten. *Phys. Rev. Lett.* **2010**, *104*, 195503.

19. Zhao, Y.; Lu, G. QM/MM study of dislocation—hydrogen/helium interactions in α-Fe. *Modell. Simul. in Mater. Sci. Eng.* **2011**, *19*, 065004.
20. Li, H.; Wurster, S.; Motz, C.; Romaner, L.; Ambrosch-Draxl, C.; Pippan, R. Dislocation-core symmetry and slip planes in tungsten alloys: Ab initio calculations and microcantilever bending experiments. *Acta Mater.* **2012**, *60*, 748–758.
21. Itakura, M.; Kaburaki, H.; Yamaguchi, M.; Okita, T. The effect of hydrogen atoms on the screw dislocation mobility in bcc iron: A first-principles study. *Acta Mater.* **2013**, *61*, 6857–6867.
22. Samolyuk, G.D.; Osetsky, Y.; Stoller, R. The influence of transition metal solutes on the dislocation core structure and values of the Peierls stress and barrier in tungsten. *J. Phys.: Condens. Matter* **2012**, *25*, 025403.
23. Romaner, L.; Razumovskiy, V.; Pippan, R. Core polarity of screw dislocations in Fe–Co alloys. *Phil. Mag. Lett.* **2014**, *94*, 334–341.
24. Ventelon, L.; Lüthi, B.; Clouet, E.; Proville, L.; Legrand, B.; Rodney, D.; Willaime, F. Dislocation core reconstruction induced by carbon segregation in bcc iron. *Phys. Rev. B: Condens. Matter* **2015**, *91*, 220102.
25. Rodney, D.; Ventelon, L.; Clouet, E.; Pizzagalli, L.; Willaime, F. Ab initio modeling of dislocation core properties in metals and semiconductors. *Acta Mater.* **2017**, *124*, 633–659.
26. Lüthi, B.; Ventelon, L.; Rodney, D.; Willaime, F. Attractive interaction between interstitial solutes and screw dislocations in bcc iron from first principles. *Comput. Mater. Sci.* **2018**, *148*, 21 – 26. doi:https://doi.org/10.1016/j.commatsci.2018.02.016.
27. Lüthi, B.; Ventelon, L.; Elsässer, C.; Rodney, D.; Willaime, F. First principles investigation of carbon-screw dislocation interactions in body-centered cubic metals. *Modelling and Simulation in Materials Science and Engineering* **2017**, *25*, 084001.
28. Kresse, G.; Hafner, J. *Phys. Rev. B: Condens. Matter* **1993**, *47*, 558.
29. Blöchl, P.E. Projector augmented-wave method. *Phys. Rev. B: Condens. Matter* **1994**, *50*, 17953–17979. doi:10.1103/PhysRevB.50.17953.
30. Kresse, G.; Joubert, D. From ultrasoft pseudopotentials to the projector augmented-wave method. *Phys. Rev. B: Condens. Matter* **1999**, *59*, 1758–1775. doi:10.1103/PhysRevB.59.1758.
31. Ventelon, L.; Willaime, F.; Clouet, E.; Rodney, D. Ab initio investigation of the Peierls potential of screw dislocations in bcc Fe and W. *Acta Mater.* **2013**, *61*, 3973 – 3985.
32. Dezerald, L.; Ventelon, L.; Clouet, E.; Denoual, C.; Rodney, D.; Willaime, F. Ab initio modeling of the two-dimensional energy landscape of screw dislocations in bcc transition metals. *Phys. Rev. B: Condens. Matter* **2014**, *89*, 024104.
33. Ventelon, L.; Willaime, F. Generalized stacking-faults and screw-dislocation core-structure in bcc iron: a comparison between ab initio calculations and empirical potentials. *Philos. Mag.* **2010**, *90*, 1063–1074.
34. Itakura, M.; Kaburaki, H.; Yamaguchi, M. First-principles study on the mobility of screw dislocations in bcc iron. *Acta Mater.* **2012**, *60*, 3698–3710.
35. Hossain, M.; Marian, J. Stress-dependent solute energetics in W–Re alloys from first-principles calculations. *Acta Mater.* **2014**, *80*, 107–117.
36. Weinberger, C.R.; Tucker, G.J.; Foiles, S.M. Peierls potential of screw dislocations in bcc transition metals: Predictions from density functional theory. *Phys. Rev. B: Condens. Matter* **2013**, *87*, 054114.
37. Alkhamees, A.; Liu, Y.L.; Zhou, H.B.; Jin, S.; Zhang, Y.; Lu, G.H. First-principles investigation on dissolution and diffusion of oxygen in tungsten. *J. Nucl. Mater.* **2009**, *393*, 508 – 512. doi:https://doi.org/10.1016/j.jnucmat.2009.07.012.
38. Lüthi, B.; Ventelon, L.; Rodney, D.; Willaime, F. Attractive interaction between interstitial solutes and screw dislocations in bcc iron from first principles. *Comput. Mater. Sci.* **2018**, *148*, 21 – 26. doi:https://doi.org/10.1016/j.commatsci.2018.02.016.
39. Johnson, D.F.; Carter, E.A. Hydrogen in tungsten: Absorption, diffusion, vacancy trapping, and decohesion. *Journal of Materials Research* **2010**, *25*, 315–327.
40. Ventelon, L.; Willaime, F.; Fu, C.C.; Heran, M.; Ginoux, I. Ab initio investigation of radiation defects in tungsten: Structure of self-interstitials and specificity of di-vacancies compared to other bcc transition metals. *Journal of Nuclear Materials* **2012**, *425*, 16–21.
41. Barouh, C.; Schuler, T.; Fu, C.C.; Jourdan, T. Predicting vacancy-mediated diffusion of interstitial solutes in α-Fe. *Phys. Rev. B* **2015**, *92*, 104102. doi:10.1103/PhysRevB.92.104102.

42. Shang, S.; Fang, H.; Wang, J.; Guo, C.; Wang, Y.; Jablonski, P.; Du, Y.; Liu, Z. Vacancy mechanism of oxygen diffusivity in bcc Fe: A first-principles study. *Corros. Sci.* **2014**, *83*, 94–102.
43. Frank, W.; Engell, H.; Seeger, A. Migration energy and solubility of oxygen in body centered cubic iron. *Z. Metallkd.* **1967**, *58*, 452–455.
44. Frank, W.; Engell, H.; Seeger, A. Solubility and interstitial migration of oxygen in bcc iron. *Trans. Metall. Soc. AIME* **1968**, *242*.
45. Li, R.; Zhang, P.; Li, X.; Zhang, C.; Zhao, J. First-principles study of the behavior of O, N and C impurities in vanadium solids. *J. Nucl. Mater.* **2013**, *435*, 71–76.
46. Ventelon, L.; Lüthi, B.; Clouet, E.; Proville, L.; Legrand, B.; Rodney, D.; Willaime, F. Dislocation core reconstruction induced by carbon segregation in bcc iron. *Phys. Rev. B: Condens. Matter* **2015**, *91*, 220102. doi:10.1103/PhysRevB.91.220102.
47. Lu. A review of modelling and simulation of hydrogen behaviour in tungsten at different scales. *Nucl. Fusion* **2014**, *54*, 086001.
48. Bakaev. Ab initio study of interaction of helium with edge and screw dislocations in tungsten. *Nucl. Instrum. Methods in Phys. Res., Sect. B: Beam Interactions with Materials and Atoms* **2017**, *393*, 150–154.
49. Zhao, Y.; Marian, J. Direct prediction of the solute softening-to-hardening transition in W–Re alloys using stochastic simulations of screw dislocation motion. *Modell. Simul. in Mater. Sci. Eng.* **2018**, *26*, 045002.

Author Contributions: LD and JM designed the research, YZ performed the DFT calculations, all authors discussed the data and participated in writing the manuscript.

Funding: The authors acknowledge support by the National Science Foundation under grant DMR-1611342.

Acknowledgments: Computer time allocations at UCLA's IDRE Hoffman2 supercomputer are acknowledged. Part of this research was performed using HPC resources from GENCI-CINES and TGCC from CEA under grants 2016-097647, A0020910156 and A0040910156

Conflicts of Interest: The authors declare no conflict of interest.